Archives of Biochemistry and Biophysics 540 (2013) 53–61

Contents lists available at ScienceDirect

Archives of Biochemistry and Biophysics

journal homepage: www.elsevier.com/locate/yabbi

Kinetic and mechanistic characterization of the glyceraldehyde 3-phosphate dehydrogenase from *Mycobacterium tuberculosis*

Brett Wolfson-Stofko, Timin Hadi, John S. Blanchard *

Department of Biochemistry, Albert Einstein College of Medicine, 1300 Morris Park Avenue, Bronx, NY 10461, United States

ARTICLE INFO

Article history:
Received 11 September 2013
and in revised form 8 October 2013
Available online 23 October 2013

Keywords:
Glyceraldehyde 3-phosphate dehydrogenase
Glycolysis
Enzyme kinetics
Kinetic isotope effects
Tuberculosis

ABSTRACT

Glyceraldehyde 3-phosphate dehydrogenase (GAPDH) is a glycolytic protein responsible for the conversion of glyceraldehyde 3-phosphate (G3P), inorganic phosphate and nicotinamide adenine dinucleotide (NAD^+) to 1,3-bisphosphoglycerate (1,3-BPG) and the reduced form of nicotinamide adenine dinucleotide (NADH). Here we report the characterization of GAPDH from *Mycobacterium tuberculosis* (Mtb). This enzyme exhibits a kinetic mechanism in which first NAD^+, then G3P bind to the active site resulting in the formation of a covalently bound thiohemiacetal intermediate. After oxidation of the thiohemiacetal and subsequent nucleotide exchange (NADH off, NAD^+ on), the binding of inorganic phosphate and phosphorolysis yields the product 1,3-BPG. Mutagenesis and iodoacetamide (IAM) inactivation studies reveal the conserved C158 to be responsible for nucleophilic catalysis and that the conserved H185 to act as a catalytic base. Primary, solvent and multiple kinetic isotope effects revealed that the first half-reaction is rate limiting and utilizes a step-wise mechanism for thiohemiacetal oxidation via a transient alkoxide to promote hydride transfer and thioester formation.

Introduction

The etiological agent of tuberculosis, *Mycobacterium tuberculosis* (Mtb), has infected nearly one-third of the human population [1]. Approximately 10% of TB-infections lead to an active, symptomatic infection that resulted in nearly 1.4 million deaths in 2011 [1]. In addition, multi-drug resistant strains have been reported in every country surveyed by the World Health Organization [1]. Yet some of the most basic metabolic enzymes of this bacterium have yet to be characterized.

Glyceraldehyde 3-phosphate dehydrogenase is a highly conserved enzyme that is utilized in central carbon metabolism by some of the most ancient forms of life [2]. GAPDH is best known for its role in glycolysis, catalyzing the reversible conversion of glyceraldehyde 3-phosphate (G3P), inorganic phosphate and NAD^+ to 1,3-bisphosphoglycerate (1,3-BPG)[1] and NADH [3]. This dehydrogenase is also unusual in that it utilizes a covalent thiohemiacetal intermediate to promote hydride transfer and catalysis [3]. The reaction of GAPDH is essential for the regeneration of the two molecules of ATP used to phosphorylate the hexose carbon source, glucose. The cleavage of fructose-1,6-bisphosphate yields the two triose phosphates that are interconverted into G3P. The oxidation of the aldehyde and substrate-level phosphorylation catalyzed by GAPDH generate NADH and the high energy carboxy-phosphoric anhydride containing 1,3-bisphosphoglycerate (1,3-BPG) that is used in the subsequent reaction catalyzed by 3-phosphoglycerate kinase to regenerate the two molecules of ATP used earlier in the glycolytic sequence. The very reactive nature of the product of GAPDH, 1,3-BPG, has recently been shown to be capable of non-enzymatic modification of proteins, including GAPDH [4].

Recent studies have also found GAPDH to be involved in a variety of cellular processes in addition to its major role in glycolysis. GAPDH has been shown to play a role in transcription, assisting in the formation of both DNA and RNA binding complexes as well as acting as a transcription factor co-activator [5–7]. Additionally, GAPDH has been identified as a microtubule-binding protein, a lactoferrin receptor, and as an apoptosis-inducer [8–11]. More information on the extra-glycolytic roles of GAPDH can be found in the review by Nichollis et al. [12].

Despite decades of work on GAPDH's from prokaryotic and eukaryotic sources, no work has been conducted on the GAPDH from *M. tuberculosis*. It was discovered early on in our work that this enzyme had significant solubility issues. This obstacle was overcome by co-transforming the Mtb-GAPDH plasmid along with

* Corresponding author. Fax: +1 718 430 8565.
E-mail addresses: blanchar@aecom.yu.edu, john.blanchard@einstein.yu.edu (J.S. Blanchard).

[1] *Abbreviations used:* 1,3-BPG, 1,3-bisphosphoglycerate; DTT, dithiolthreitol; D-G3P, D-glyceraldehyde 3-phosphate; 1-[^{2}H]D-G3P, 1-[^{2}H]D-glyceraldehyde 3-phosphate; G3P, Glyceraldehyde 3-phosphate; GAPDH, Glyceraldehyde 3-phosphate dehydrogenase; HEPES, *N*-(2-hydroxyethyl)piperazine-*N*′-(2-ethanesulfonic acid); IAM, iodoacetamide; LB, Luria–Bertani; MES, 2-(*N*-morpholino)ethanesulfonic acid; MKIE, multiple kinetic isotope effect; NAD^+, nicotinamide adenine dinucleotide; NADH, reduced nicotinamide adenine dinucleotide; Ni-NTA, nickel nitriloacetic acid; PCR, polymerase chain reaction; PKIE, primary isotope effect; SDS–PAGE, sodium dodecyl sulfate–polyacrylamide gel electrophoresis; SKIE, solvent kinetic isotope effect; TAPS, *N*-[tris(hydroxymethyl)methyl]-3-aminopropanesulfonic acid.

0003-9861/$ - see front matter © 2013 Elsevier Inc. All rights reserved.
http://dx.doi.org/10.1016/j.abb.2013.10.007

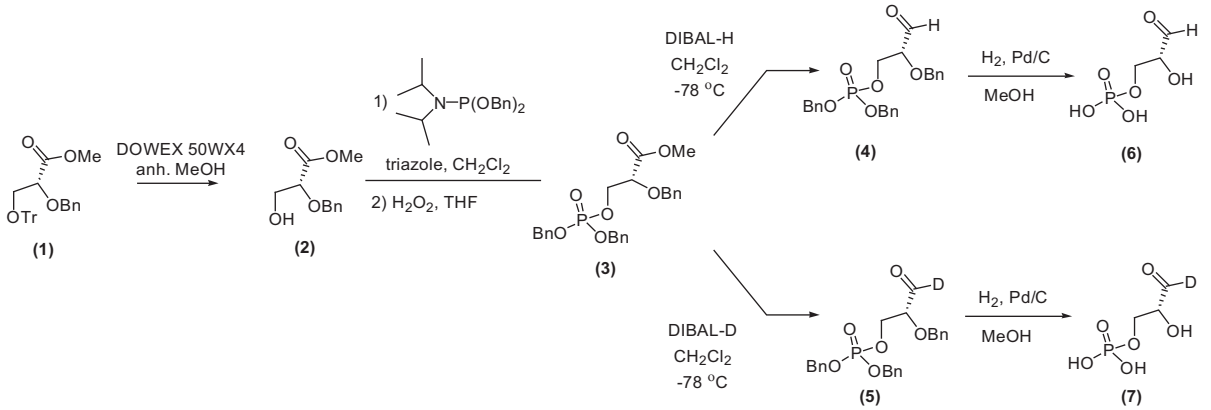

Scheme 1. Synthesis of D-glyceraldehyde 3-phosphate and [1-^{2}H]D-glyceraldehyde 3-phosphate.

a plasmid expressing the chaperones GroEL/GroES [13]. These chaperones are believed to create an environment suitable for proper folding yielding soluble and active Mtb-GAPDH [13]. In this study, we report the first successful purification and mechanistic evaluation of Mtb-GAPDH using steady-state kinetics, pH-rate profiles, isotope effects and mutagenesis to elucidate both the kinetic and chemical mechanism of Mtb-GAPDH.

Materials and methods

Materials

All chemicals were purchased from Sigma–Aldrich unless otherwise noted. The Mtb-GAPDH gene was cloned into the Novagen pET-28a(+) vector. The GroEL/GroES plasmid was a gift from the Shrader Lab [13]. Primers were purchased from Invitrogen. All cloning enzymes and T7 competent *Escherichia coli* were purchased from New England Biolabs. Complete EDTA-free protease inhibitor cocktail and DNase were purchased from Roche. 99.9% deuterated water was purchased from Cambridge Isotope Laboratories.

Cloning, expression and purification of Mtb-GAPDH

The *M. tuberculosis gap* gene (Rv1436) was PCR amplified from the Erdman strain with a forward primer 5′-GGAATTCCATATGGTG ACGGTCCGAGTAGGC-3′ and a reverse primer 5′-GTCGGCAAGTCGC TCTAGAAGCTTGGG-3′. NdeI and HindIII restriction sites were used for forward and reverse primers, respectively. The PCR fragment was ligated into the pET28a(+) vector encoding for a N-terminal His_6-tag. The plasmid was then sequenced and confirmed. The Mtb-GAPDH-containing plasmid was co-transformed along with the GroEL/GroES plasmid into T7 Express *E. coli* competent cells. Kanamycin (35 μg/mL) and tetracyclin (6 μg/mL) were used for selection. Cultures were grown in LB broth at 30 °C and induced with 500 μM IPTG at an A_{600} of ~0.6–0.8 and then grown overnight at 18 °C. Cells were harvested by centrifugation and stored at −20 °C. The pellets were resuspended in 25 mM HEPES (pH 7.5) containing 300 mM NaCl, 10 mM imidazole, and 1 mM NAD^+. Cells were lysed using an EmulsiFlex-C3 and centrifuged to remove cellular debris. The clear supernatant was then added to a Ni^{2+}-NTA agarose column and eluted with a linear imidazole gradient (10 mM-250 mM). Fractions containing Mtb-GAPDH were pooled and dialyzed into 25 mM HEPES (pH 7.5) containing 300 mM NaCl, 1 mM NAD^+ and 5% glycerol then concentrated and stored at −20 °C in 12.5% glycerol.

Construction and expression of Mtb-GAPDH mutants C158A, C162A and H185A

Mtb-GAPDH/pET28a was used as a template to generate C158A, C162A and H185A mutants. The mutants were constructed by overlap mutagenesis [14]. The mutation has been underlined in the following sequences. The forward primer for C158A was 5′-CTCCAATGCGTCGGCCACCACGAACTGCC-3′ and the reverse primer was 5′-GGCAGTTCGTGGTGGCCGACGCATTGGAG-3′. The forward primer for C162A was 5′-GTGCACCACGAACGCCCTTGCGCCGCTGG-3′ and the reverse primer was 5′-CCAGCGGCGCAAGGGCGTTCGTGG TGCAC-3′. The forward primer for H185A was 5′-GATGACCAC-CATCGCCGCCTACACTCAGG-3′ and the reverse primer was 5′-CCTG AGTGTAGGCGGCGATGGTGGTCATC-3′. DNA sequencing was used to confirm the described mutations. Each mutant was expressed and purified in the same manner as wild-type Mtb-GAPDH.

Protein concentration

Protein concentration was determined using Bio-Rad Bradford protein assay using bovine serum albumin as a standard.

Measurement of enzymatic activity

Enzymatic activity was measured spectrophotometrically by monitoring the conversion of NAD^+ to NADH at 340 nm. Reactions were conducted in 50 mM HEPES, pH 8 including substrates NAD^+, Na_2AsO_4, and DL-G3P in a total volume of 500 μL. Reactions were initiated by the addition of Mtb-GAPDH. Initial velocities were measured before 10% conversion of substrate to product had occurred and initial rates were calculated using the molar extinction coefficient of NADH (ε_{340} = 6220 M^{-1} cm^{-1}) and the total enzyme concentration.

The measurements of kinetic isotope effects were conducted in the same manner with a few differences. We synthesized and utilized the individual stereoisomers, [1-^{1}H]D-glyceraldehyde 3-phosphate (1-[^{1}H]D-G3P) and [1-^{2}H]D-glyceraldehyde 3-phosphate (1-[^{2}H]D-G3P) for these studies. Concentrations of 1-[^{1}H]D-G3P and 1-[^{2}H]D-G3P were determined enzymatically using excess NAD^+ and arsenate.

Synthesis of D-glyceraldehyde 3-phosphate and [1-^{2}H]D-glyceraldehyde 3-phosphate

Briefly, the known compound, methyl (*R*)-2-benzyloxy-3-trityloxypropanoate (**1**), was synthesized from commercially available methyl 2,3-*O*-isopropylidene-D-glycerate according to previously

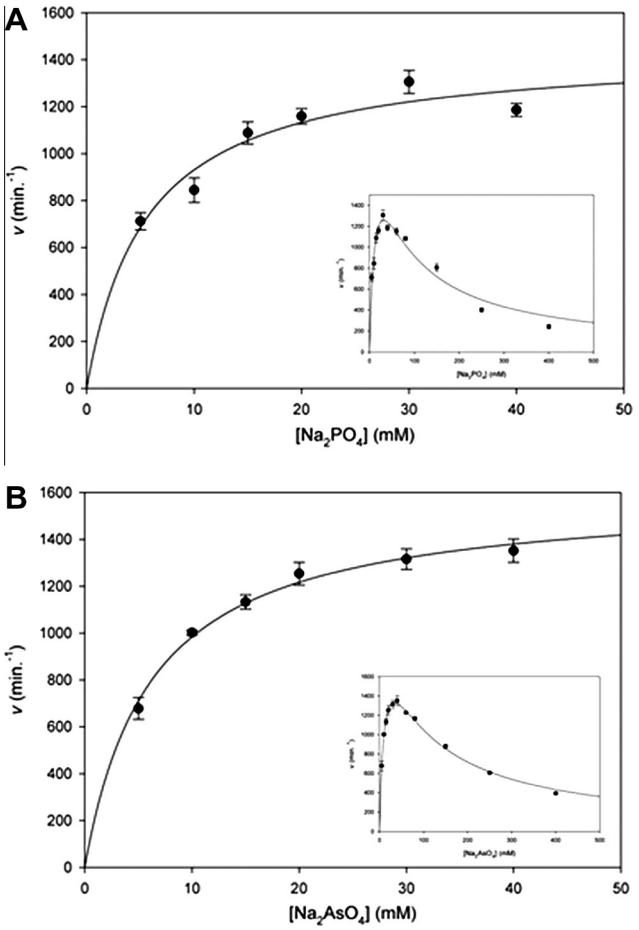

Fig. 1. Michaelis–Menten experiments with Mtb-GAPDH utilizing phosphate (A) or arsenate (B) as the varying substrates with 50 mM HEPES, pH 8, and saturating concentration of G3P and NAD^+. Data were fit to Eq. (2). Substrate inhibition profiles utilizing phosphate (inset A) or arsenate (inset B) with 50 mM HEPES, pH 8 and saturating concentration of G3P and NAD^+. Data were fit to Eq. (1).

published procedures [15]. The 3-*O*-trityl ether was removed to generate compound **2** bearing a free hydroxyl group at the C3 position (Scheme 1). This hydroxyl group was phosphorylated using a phosphoramidite coupling reagent to generate the common intermediate compound **3** that was used for the synthesis of both D-glyceraldehyde 3-phosphate and [1-^{2}H]D-glyceraldehyde 3-phosphate. To generate the aldehyde at the C1 position, compound **3** was treated with DIBAL-H or DIBAL-D to generate compounds **4** and **5**, respectively. D-Glyceraldehyde 3-phosphate (**6**) and [1-^{2}H]D-glyceraldehyde 3-phosphate (**7**) were then generated through hydrogenolysis (1 atm H_2, Pd/C catalyst) of the benzyl-protected compounds. Further experimental detail and NMR spectra can be found in the Supplementary Information.

Initial velocity studies

Data were fit using SigmaPlot 11.0. All points are the mean of experimental duplicates and the error bars are plus/minus one half of the difference between the experimental duplicates. Substrate inhibition curves were determined and fitted to Eq. (1) for linear substrate inhibition

$$v = VS/(K_m + S + S^2/K_i) \quad (1)$$

where v is the velocity, S is the concentration of substrate and K_i is the substrate inhibition constant. Initial kinetic parameters were estimated by saturating two substrates while varying the concentration of the third. These rates were fit to Eq. (2)

$$v = (VS)/(k_m + S) \quad (2)$$

where V is the maximal velocity and S is the concentration of the varied substrate. Initial velocity studies were conducted by saturating

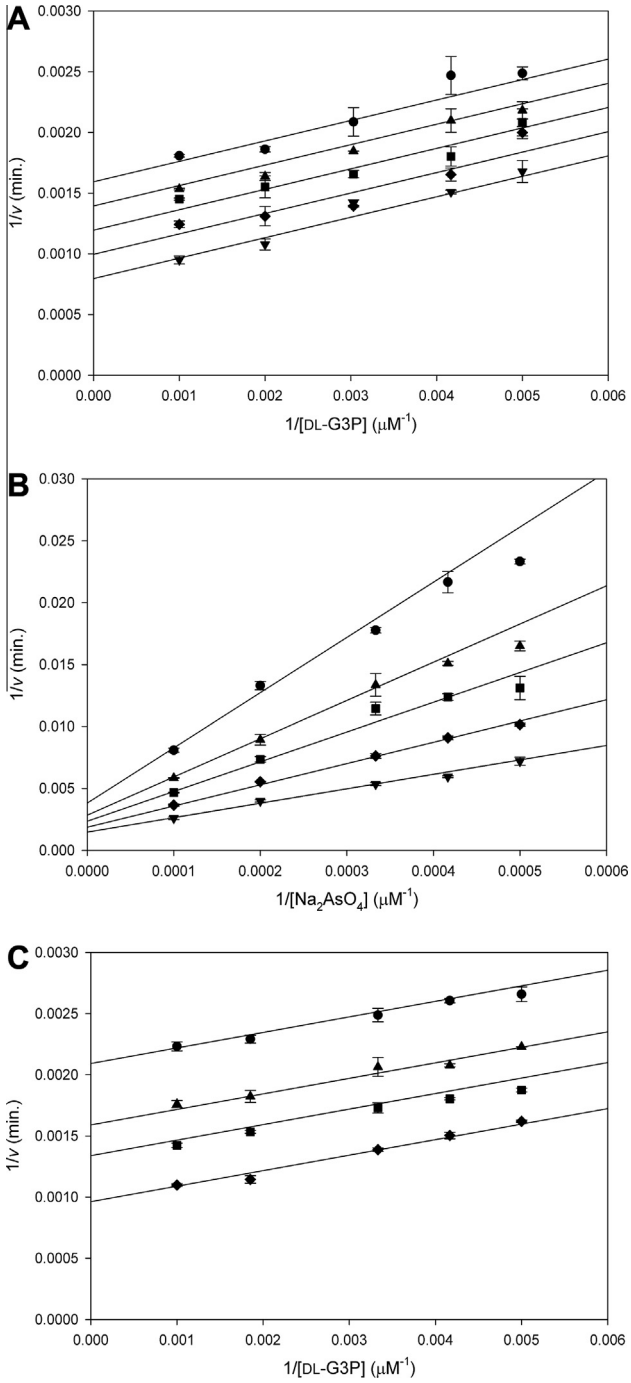

Fig. 2. Initial velocity studies. (A) Initial rate data were obtained by varying concentrations of G3P and fixed, variable concentrations of NAD^+ at 24 (●), 30 (▲), 40 (■), 60 (♦) and 120 μM (▼) and high non-inhibitory concentrations of Na_2AsO_4. The data were fit to Eq. (4). (B) Initial rate data were obtained by varying concentrations of Na_2AsO_4 and fixed, variable concentrations of NAD^+ at 20 (●), 30 (▲), 40 (■), 60 (♦) and 100 μM (▼) at saturating concentrations of G3P. The data were fit to Eq. (3). (C) Initial rate data were obtained by varying concentrations of G3P and fixed, variable concentrations of Na_2AsO_4 at 2 (●), 3 (▲), 4 (■), and 8 mM (♦) at saturating concentrations of NAD^+. The data were fit to Eq. (4).

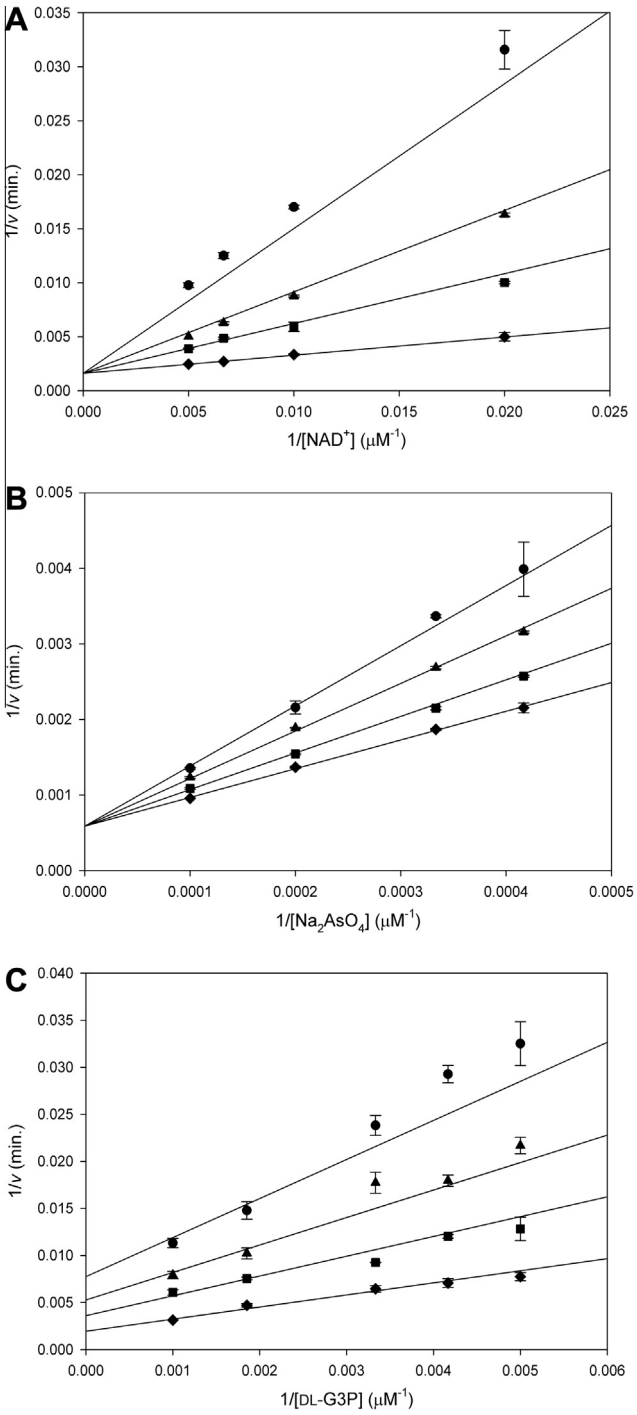

Fig. 3. Product inhibition studies. (A) Initial rate data were obtained at varying concentrations of NAD^+ and fixed, variable concentrations of NADH at 0 (♦), 25 (■), 50 (▲), and 100 μM (●). The data were fit to Eq. (5). (B) Initial rate data were obtained at varying concentrations of Na_2AsO_4 and fixed, variable concentrations of NADH at 0 (♦), 10 (■), 24 (▲), and 40 μM (●). The data were fit to Eq. (5). (C) Varying concentrations of G3P and fixed, variable concentrations of NADH at 0 (♦), 20 (■), 40 (▲), and 70 μM (●). The data were fit to Eq. (7).

with one substrate, fixing the concentration of another, and varying the concentration of the third. The results were fitted for intersecting and parallel patterns using Eqs. (3) and (4), respectively

$$v = (VAB)/(K_{ia}K_b + K_aB + K_bA + AB) \quad (3)$$

$$v = (VAB)/(K_aB + K_bA + AB) \quad (4)$$

where V is the maximal velocity, A and B are substrate concentrations, K_a and K_b are the respective Michaelis constants for each of the substrates, and K_{ia} is the inhibition constant for substrate A. Product inhibition was performed using reduced nicotinamide adenine dinucleotide (NADH) as an inhibitor. Data was obtained at variable concentrations of NAD^+, G3P or arsenate at several fixed concentrations of NADH. The data were fit to competitive, uncompetitive, and noncompetitive inhibition using Eqs. (5)–(7), respectively

$$v = (VS)/[K_m(1 + I/K_{is}) + S] \quad (5)$$

$$v = (VS)/[K_m + S(1 + I/K_{ii})] \quad (6)$$

$$v = (VS)/[K_m(1 + I/K_{is}) + S(1 + I/K_{ii})] \quad (7)$$

where S is the varied substrate concentration, I is the inhibitor concentration, K_{is} is the inhibition constant for the slope, K_{ii} is the inhibition constant for the intercept, and K_m is the Michaelis constant for the substrate S.

pH dependence studies

The pH dependence of the kinetic parameters was determined in 50 mM concentrations of buffers at various pH values and using the following structurally related buffers at the pH values noted in parentheses: MES (pH 5–6.5), HEPES (pH 6.5–8), TAPS (pH 8–10). The pH profile was determined varying either G3P or Na_2AsO_4 with other substrates held saturating. The data were fit to Eq. (8)

$$\log k = \log[c/(1 + K_b/10^{-pH} + 10^{-pH}/K_a)] \quad (8)$$

where c is the pH-independent plateau value and K_a and K_b are dissociation constants of the ionizing groups.

Inactivation studies

Inactivation studies were performed using iodoacetamide (IAM) as an inactivator. Enzyme activities were measured for native Mtb-GAPDH every 15-min and every 20-min for Mtb-GAPDH C162A at varying concentrations of IAM. Kinetic constants were calculated as described by Kitz and Wilson [16]. Briefly, relative inhibition was determined by comparing the rates of time-matched samples exposed to varying concentrations of IAM to control samples lacking IAM. The results were plotted on a logarithmic scale versus time and the slopes were determined by linear regression. The values of the slopes represent the inactivation rate constants and were used to calculate the half-life of the inactivation ($k_{inactivation} = 0.693/t_{1/2}$). A Kitz–Wilson plot was produced using

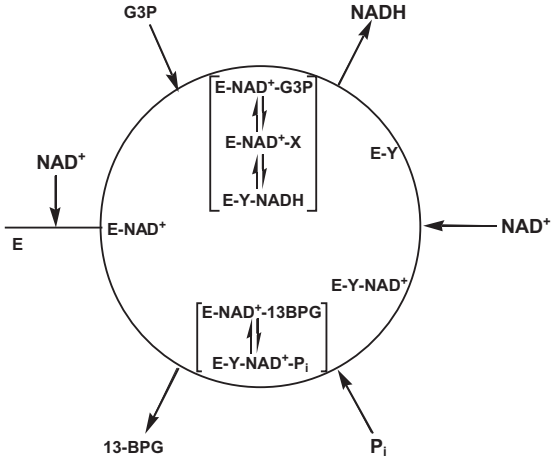

Scheme 2. Proposed kinetic mechanism of Mtb-GAPDH.

the calculated half-lives as the *y*-axis and the reciprocal of the inhibitor concentration as the *x*-axis [16]. Values for K_i and $k_{inactivation}$ were determined from the negative reciprocal of the *x*-intercept and reciprocal of the *y*-intercept, respectively.

Kinetic isotope effects

Solvent kinetic isotope effects were determined at varying concentrations of either D-G3P or Na_2AsO_4 while the other substrates were kept at saturating concentrations in H_2O or 90% D_2O. A viscosity control of 9% glycerol was performed and revealed no effect on V or V/K_m [17]. The data were fit to Eq. (9)

$$v = (VS)/[K_A(1 + F_i(E_{V/K} - 1)) + S(1 + F_i(E_V - 1))] \quad (9)$$

where V is the maximal velocity, S is the substrate concentration, $E_{V/K}$ is the effect on k_{cat}/K_m, E_V is the effect of k_{cat} and F_i is the fraction of the isotope ($F_i = 0$ for H_2O and $F_i = 0.9$ for D_2O). A proton inventory was then conducted using saturating conditions of substrates while varying D_2O concentrations from 0% to 90%. The results were fit to a linear equation.

Primary and multiple kinetic isotope effects were determined at varying concentrations of either [1-^{1}H]D-G3P or [1-^{2}H]D-G3P while other substrates were kept at saturating conditions in either H_2O or 90% D_2O. The results were fitted to Eq. (9).

Results and discussion

Cloning, expression and purification

Mtb-GAPDH was PCR amplified then cloned into the pET28a expression vector encoding a N-terminal His_6-tagged Mtb-GAPDH. Sequencing confirmed that no mutations were introduced during the cloning process. Initial expression studies revealed that Mtb-GAPDH was insoluble under normal conditions. Co-transformation of the Mtb-GAPDH plasmid along with a GroEL/GroES plasmid yielded soluble and active protein. After purification and dialysis, the final protein preparation was >95% pure as determined by SDS–PAGE. The addition of 1 mM NAD^+ to the sonication and purification buffers was essential to maintain the activity of GAPDH (data not shown).

Measurement of enzyme activity

The activity of Mtb-GAPDH was determined using a direct spectrophotometric assay measuring the conversion of NAD^+ into NADH at 340 nm. $NADP^+$ was screened as an alternate substrate for NAD^+ but no activity could be demonstrated. Na_2AsO_4 was substituted for the normal Mtb-GAPDH endogenous substrate, Na_2PO_4, to prevent the reverse reaction. This substitution yields the product, 1-arseno-3-phosphoglycerate, which is rapidly hydrolyzed. Na_2AsO_4 exhibited kinetic constants ($K_m = 6.2 \pm 0.6$ mM, $V = 1590 \pm 40$ min.$^{-1}$) similar to Na_2PO_4 ($K_m = 6 \pm 1$ mM, $V = 1450 \pm 70$ min.$^{-1}$) (Fig. 1A and B). These studies also revealed that both Na_2PO_4 and Na_2AsO_4 cause linear substrate inhibition at concentrations higher than 30 mM (Fig. 1A and B, insets), presumably due to competition with the phosphate binding site for G3P. Fits of these data to Eq. (1) yielded K_i values of 60 ± 10 and 93 ± 7 mM for Na_2PO_4 and Na_2AsO_4, respectively.

Kinetic mechanism

Initial velocity studies were conducted to elucidate the kinetic mechanism of Mtb-GAPDH. Commercially available DL-G3P was used as a substrate for these studies due to the laborious procedures required to synthesize the single D-G3P stereoisomer. Consequently, concentration values reported herein are for the DL-G3P mixture and presumed to be two times the value for D-G3P alone. Double-reciprocal plots yielded a series of parallel lines when varying G3P concentration at several fixed NAD^+ concentrations and an optimal, but not saturating concentration of Na_2AsO_4 (Fig. 2A). Because the concentration of Na_2AsO_4 was chosen to avoid substrate inhibition, reported values of V may slightly underestimate the actual value. Fitting these data to Eq. (4) yielded $V = 1670 \pm 90$ min.$^{-1}$, $K_{G3P} = 280 \pm 30$ μM and $K_{NAD+} = 40 \pm 4$ μM. Varying Na_2AsO_4 concentrations at several fixed NAD^+ concentrations resulted in a series of intersecting lines that when fit to Eq. (3) yielded $K_{Na2AsO4} = 3.9 \pm 1.5$ mM, and $K_{NAD+} = 70 \pm 20$ μM (Fig. 2B). Varying G3P concentrations at several fixed concentrations of Na_2AsO_4 resulted in a series of parallel lines that when fit to Eq. (4) yielded $V = 1710 \pm 60$ min.$^{-1}$ and $K_{Na2AsO4} = 5.1 \pm 0.3$ mM (Fig. 2C). To elucidate the binding order of substrates and product release, product inhibition studies were performed. NADH was determined to exhibit competitive inhibition versus both NAD^+ and Na_2AsO_4 (Fig. 3A and B). Fits of these data to Eq. (5) yielded K_i values of 14 ± 1 μM and 37 ± 1 μM versus NAD^+ and Na_2AsO_4, respectively. NADH exhibited noncompetitive inhibition versus G3P and when fit to Eq. (7) yielded $K_{ii} = 24 \pm 5$ and $K_{is} = 31 \pm 7$ μM (Fig. 3C).

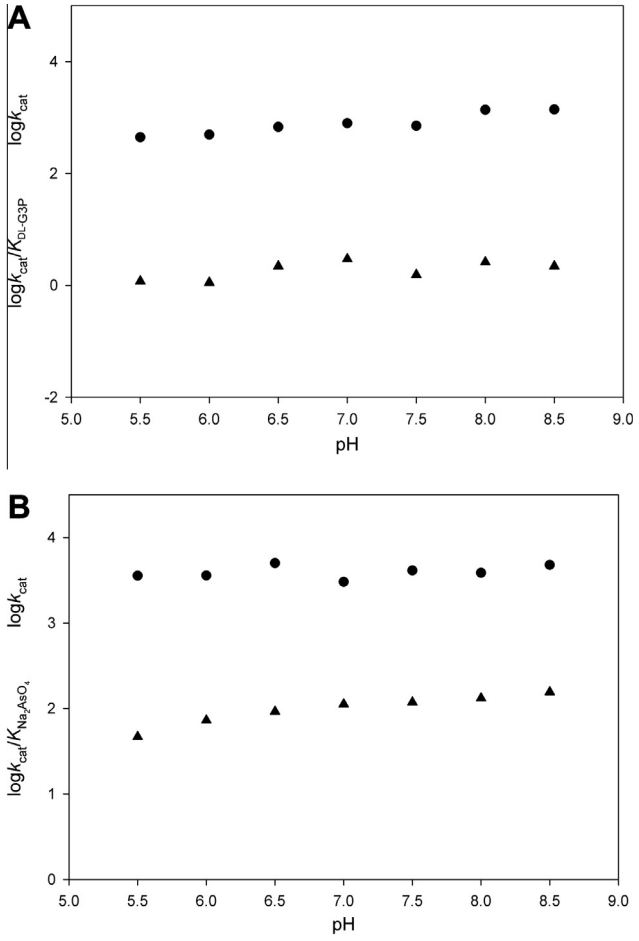

Fig. 4. pH dependence studies for Mtb-GAPDH. (A) Experiments were performed by varying concentrations of G3P at saturating conditions for all other substrates at pH values from 5.5 to 8.5. Individual curves at each pH value were fit to Eq. (2), and the k_{cat} and k_{cat}/K_{G3P} values plotted. (B) Experiments were performed by varying concentrations of AsO_4 at saturating conditions for all other substrates at pH values from 5.5 to 8.5. Individual curves at each pH value were fit to Eq. (2), and the k_{cat} and k_{cat}/K_{G3P} values plotted.

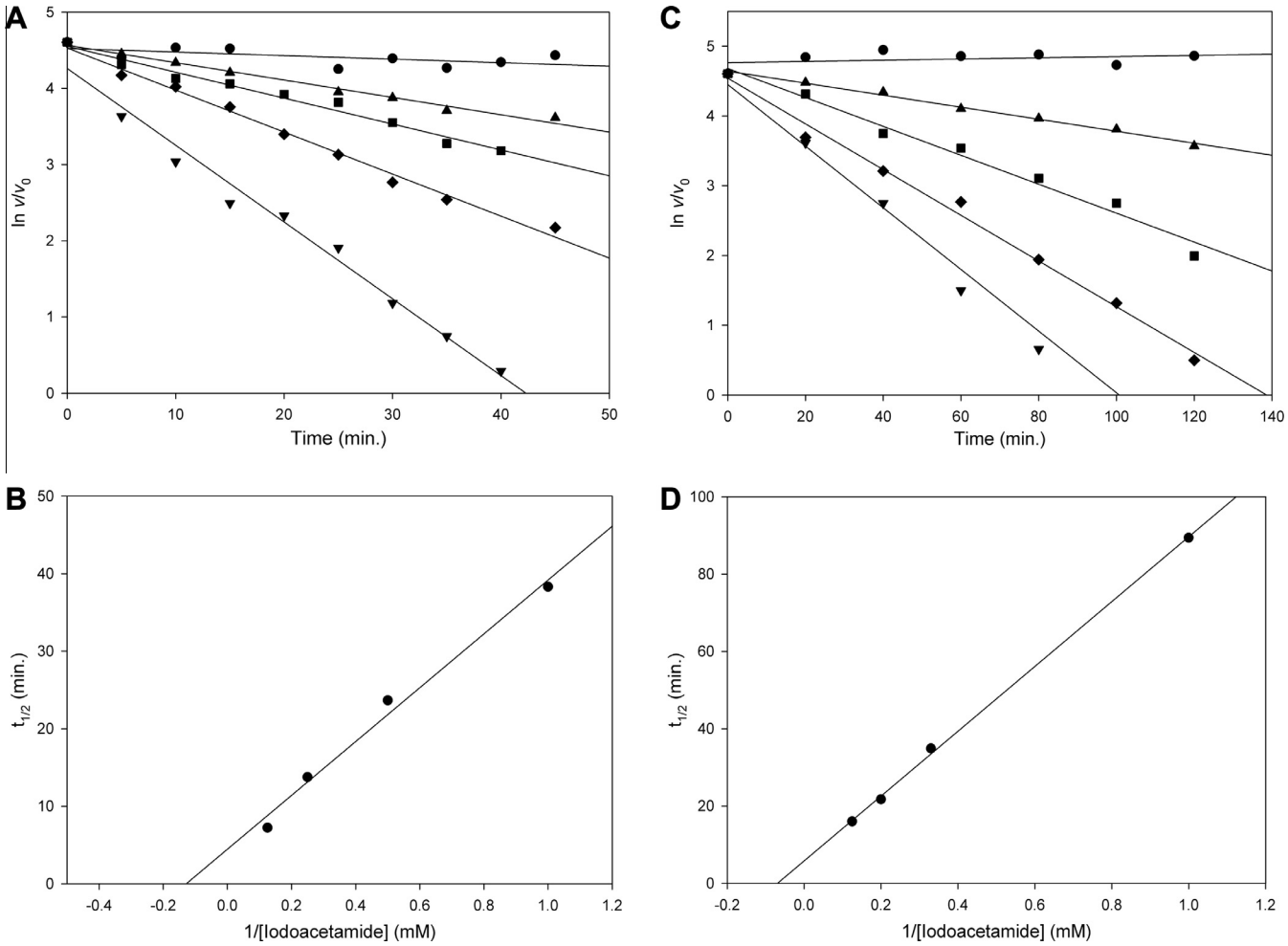

Fig. 5. Inactivation of native Mtb-GAPDH with iodoacetamide. (A) Time- and concentration-dependent inactivation at [IAM] = 0 (●), 1 (▲), 2 (■), 4 (♦), 8 mM (▼) and (B) Kitz–Wilson re-plot. Inactivation of C162A Mtb-GAPDH with iodoacetamide. (C) Time- and concentration-dependent inactivation at [IAM] = 0 (●), 1 (▲), 3 (■), 5 (♦), 8 mM (▼) and (D) Kitz–Wilson re-plot.

Together, these data are consistent with an unusual kinetic mechanism in which the free enzyme is in reality the E-NAD^+ complex. This is supported by both the parallel line initial velocity pattern observed when G3P and NAD^+ are varied (requiring a product to be released between them) and the requirement of NAD^+ for stability. G3P first binds to the E-NAD^+ complex, and reacts with the active site C158 to generate the thiohemiacetal intermediate (E-NAD^+-X in Scheme 2). Hydride transfer to NAD^+ generates NADH and the enzyme thioester intermediate (E-Y-NADH in Scheme 2), which undergoes a "nucleotide exchange" reaction to generate the thioester–NAD^+ complex (E-Y-NAD^+). Binding of phosphate and phosphorolysis of the thioester generates the product, 1,3-bisphosphoglycerate, leaving the enzyme with NAD^+ bound and ready to react with another G3P molecule. A similar "nucleotide exchange" kinetic scheme was reported for GAPDH from both rabbit and pig muscle [3,18,19].

pH dependence studies

To determine which enzyme residues are required for catalytic function, pH dependence studies were performed. Control experiments were conducted to determine the stability of Mtb-GAPDH. These studies limited our profile to the pH range of 5.5–8.5. Experiments varying G3P concentrations at saturating concentrations of NAD^+ were used to evaluate the effect of ionizations on $\log k_{cat}$ and $\log k_{cat}/K_{G3P}$. This experiment yielded no detectable change in either kinetic parameter over this pH range (Fig. 4A), suggesting that the ionization of the active site cysteine and histidine residues [20] implicated in the first chemical reaction (thiohemiacetal formation and hydride transfer to generate the thioester) were

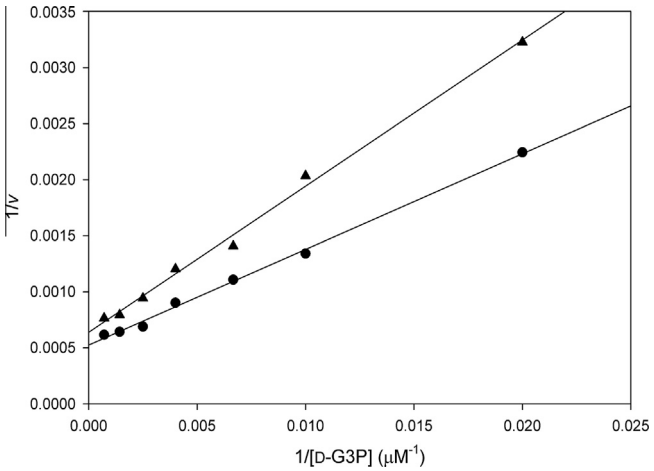

Fig. 6. Primary kinetic isotope effects. Primary kinetic isotope effects were determined using 1-[^{1}H]D-G3P (●) and 1-[^{1}H]D-G3P (▲) at saturating concentrations of other substrates. The data were fitted to Eq. (9).

outside of the experimental range. Unfortunately, due to enzyme instability outside of this pH range we were unable to probe the enzymatic reaction at pH's that were closer to the pK_1 and pK_2 values previously reported by Polgár for NAD^+-bound GAPDH (5.2 and 8.9, respectively) [20]. Similar experiments varying Na_2AsO_4 to probe for ionizations implicated in the phosphorolysis reaction also yielded no evidence for enzyme side chain participation (Fig. 4B).

Studies with GAPDH homologs have demonstrated the essential role of an active site cysteine responsible for the formation of the thioacyl intermediates [3,18,21]. The active site cysteine has been reported to form a thiolate-imidazolium ion-pair with an active site histidine that increases the reactivity of the cysteine [3,20,22–24]. These residues have been identified through sequence alignment to correspond to C158 and H185 in Mtb-GAPDH. The lack of any pH dependence of the kinetic parameters in the pH range tested for Mtb-GAPDH is likely due to the unusual kinetic mechanism and the requirement of bound NAD^+ (or NADH) for stability and throughout the catalytic cycle. Crystal structures have shown the binding of NAD^+ to induce a conformational change in the GAPDH of *Bacillus stearothermophilus* leading to a repositioning of active site residues favoring the stabilization of a thiolate-imidazolium pair [25]. Polgár has theorized that the formation of the thiolate-imidazolium pair in GAPDH would lead to altered p*K* values that would appear outside the pH range tested [20]. Given our inability to assess the required appropriate ionization state of residues implicated in catalysis by variations in external pH, mutagenesis studies were conducted to probe the roles of C158, C162 and H185.

Mutagenesis and inactivation studies

In order to verify the essential role of C158 in catalysis, kinetic inactivation studies were performed. Iodoacetamide (IAM), an irreversible, cysteine-specific alkylator was used to probe the role of the active site cysteines C158 and C162A in catalysis. Fig. 5A illustrates the inhibition of Mtb-GAPDH with IAM in both a time- and concentration-dependent manner. A Kitz–Wilson re-plot gave a $k_{inactivation}$ and K_i of IAM of 0.16 $min.^{-1}$ and 7.8 mM, respectively (Fig. 5B). This data supports the proposed function of an active site cysteine in catalysis, as previously reported in other GAPDH homologs [3,19,21].

The C158A, C162A and H185A mutant forms of Mtb-GAPDH were constructed and purified in order to determine their role in catalysis. The C158A mutant was inactive, but the C162A mutant exhibited a comparable *V* to native Mtb-GAPDH and only a 2-fold increase in the value of K_{G3P} (data not shown). Time- and concentration-dependent inactivation studies with IAM were conducted with C162A to verify that acetamidation of C158, and not C162 was responsible for the loss of activity (Fig. 5C). A Kitz–Wilson re-plot gives a $k_{inactivation}$ and K_i of IAM of 0.12 $min.^{-1}$ and 14 mM, respectively, comparable to the wild-type enzyme (Fig. 5D). The H185A mutant was also inactive suggesting that C158 is the active site nucleophile reacting with the aldehyde group of G3P to generate the thiohemiacetal and that H185 is additionally required to either stabilize thiolate anion formation or act as a catalytic acid/base group.

Kinetic isotope effects

Studies of kinetic isotope effects were performed to identify the rate-limiting chemical steps. In order to measure the primary kinetic isotope effect on the Mtb-GAPDH catalyzed reaction, the synthesis of a single stereoisomer of glyceraldehyde 3-phosphate ([1-^{1}H]D-G3P) and [1-^{2}H]D-glyceraldehyde 3-phosphate ([1-^{2}H]D-G3P) was performed. Using these compounds, only modest isotope effects were observed on *V* ($^DV_{G3P} = 1.2 \pm 0.1$) and *V*/*K* ($^DV/K_{G3P} = 1.5 \pm 0.2$, Fig. 6). The expression for $^DV/K$ includes rate constants from the binding of G3P to the E-NAD^+ complex to the first irreversible step, which we suggest is NADH release (Scheme 2). The value of $^DV/K_{G3P}$ is significantly smaller than one would expect for a hydride transfer reaction, and indicates that G3P is sticky. Certainly the formation of a covalent thiohemiacetal would contribute to a high commitment factor for this substrate. This

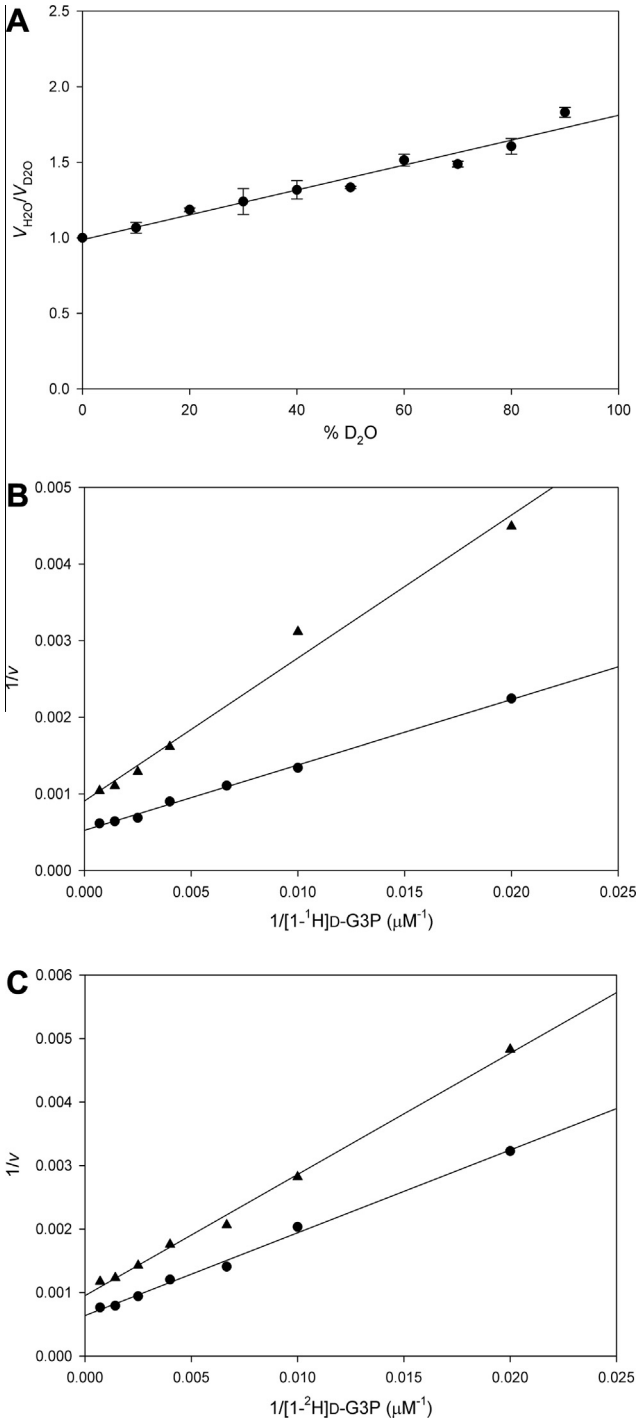

Fig. 7. Solvent kinetic isotope effects. (A) Proton inventory from 0 to 90 atom% D_2O at saturating conditions of all substrates. (B) Solvent kinetic isotope effects determined using 1-[^{1}H]D-G3P at saturating concentrations of other substrates in H_2O (●) and 90% D_2O (▲). The data were fit to Eq. (9). (C) Multiple kinetic isotope effects determined using 1-[^{2}H]D-G3P at saturating concentrations of other substrates in H_2O (●) and 90% D_2O (▲). The data were fit to Eq. (9).

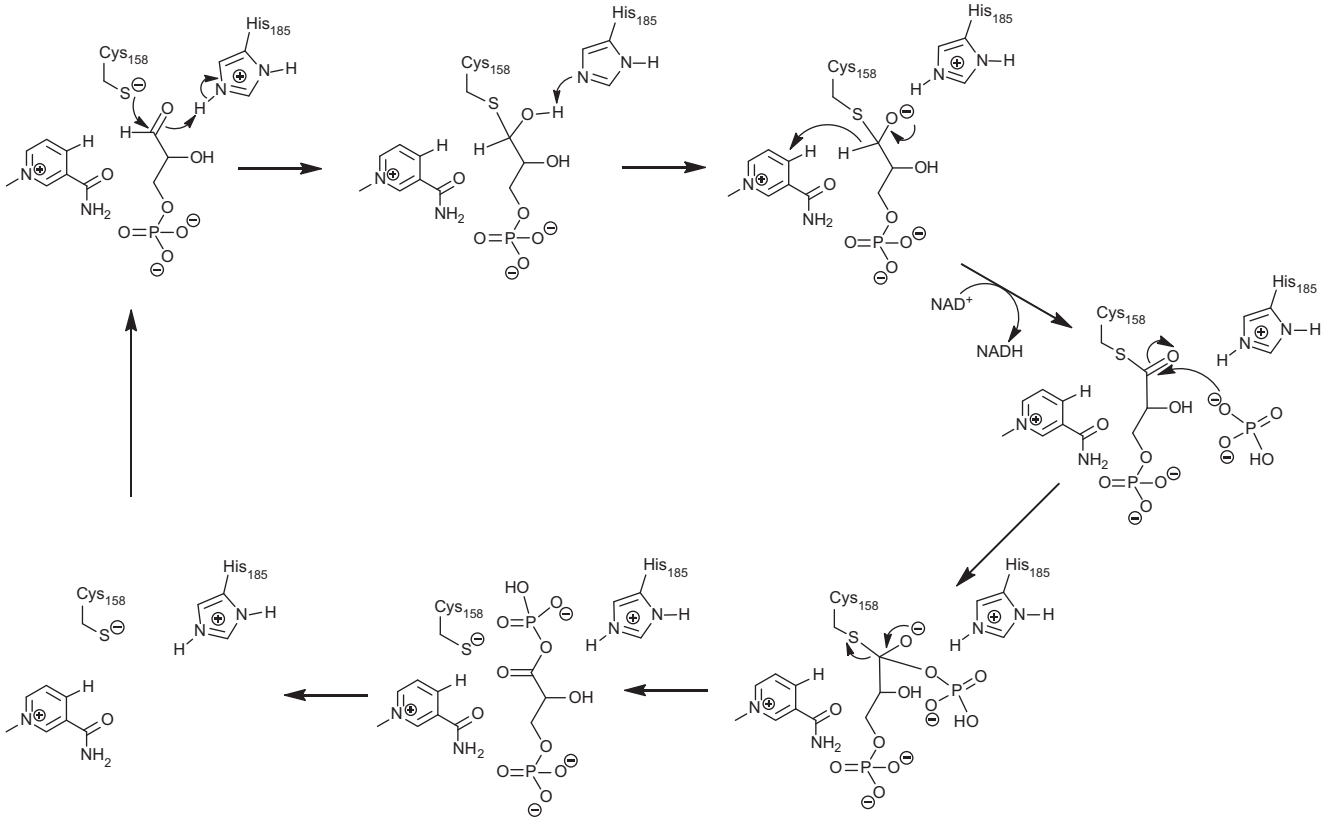

Scheme 3. Proposed chemical mechanism of Mtb-GAPDH.

chemistry also results in there being a small (*ca.* 1.2) inverse equilibrium effect on the formation of the thiohemiacetal when using [1-^{2}H]$_D$-G3P versus [1-^{1}H]$_D$-G3P due to the change in hybridization from sp^2 to sp^3. Together these data suggest that the hydride transfer is only partially rate-limiting in the chemical oxidation of the covalently-bound thiohemiacetal. The even lower value of ^DV may reflect additional rate limitation by product release. These results are quantitatively similar to those obtained under similar experimental conditions with rabbit muscle GAPDH [18].

In order to probe additional chemical steps in the oxidation reaction, solvent kinetic isotope effects (SKIE) were used to investigate the potential rate-limiting nature of proton transfer steps. A proton inventory was conducted under "pseudo-*V*" conditions (5–10 times K_m values for G3P and NAD^+ and maximal, but not substrate inhibitory concentrations of arsenate) in 10% increments of D_2O from 0% to 90%. This experiment yielded a linear, normal dependence of the rate on solvent isotopic composition, indicative of a single solvent-derived proton being involved in the oxidative half-reaction (Fig. 7A). The extrapolated magnitude of "^{D2O}V" was approximately 1.7.

Experiments performed with 1-[^{1}H]$_D$-G3P in H_2O and 90% D_2O at pH 8 yielded values of ^{D2O}V of 1.7 ± 0.1 and $^{D2O}V/K_{G3P}$ of 2.5 ± 0.4, respectively, (Fig. 7B). As is the case for the primary KIE, $^{D2O}V/K_{G3P}$ includes rate constants from the binding of G3P to the release of NADH. In the steps that represent the oxidation of the thiohemiacetal (Scheme 3), the formation of the thiohemiacetal is accompanied by protonation of the carbonyl oxygen. Oxidation and hydride transfer will occur only after deprotonation of the alcohol, and it is this step that is the most likely source of the single-proton solvent KIE. The magnitude of V/K_{G3P} suggests that this step is slow, and that the relatively rate-limiting formation of the alkoxide by His185-assisted deprotonation promotes a more rapid hydride transfer to NAD^+ from the thiohemiacetal alkoxide. This interpretation is further supported by the inactivity of H185A, as has been previously suggested [24]. The smaller magnitude of ^{D2O}V suggests that steps after the oxidative half-reaction contribute to overall rate limitation, as was discussed for the primary KIE.

Oxidation of secondary alcohols can presumably be carried out in either a concerted (deprotonation-hydride transfer) or stepwise manner. Theory has been developed that allows the discrimination of these two mechanisms using multiple kinetic isotope effects [26]. We elected to perform multiple kinetic isotope effect (MKIE) experiments examining the effect of substrate deuteration on the solvent KIE, since the solvent KIE's are larger and more likely to reveal statistically significant differences, if present. Using 1-[^{2}H]$_D$-G3P in H_2O and 90% D_2O at pH 8, the solvent kinetic isotope effects on $^{D2O}V_{1\text{-}[2H]_D\text{-}G3P}$ was 1.6 ± 0.1 and $^{D2O}V/K_{1\text{-}[2H]_D\text{-}G3P}$ was 1.4 ± 0.2 (Fig. 7C). ^{D2O}V using either 1-[^{1}H]$_D$-G3P or 1-[^{2}H]$_D$-G3P were equivalent (1.6–1.7) and equal to the extrapolated value from the proton inventory experiment. However, $^{D2O}V/K_{1\text{-}[2H]_D\text{-}G3P}$ was significantly smaller than when 1-[^{1}H]$_D$-G3P was used as substrate (1.4 versus 2.5). This suggests that the two isotopic perturbants affect different steps (alkoxide formation or hydride transfer) and that as the hydride transfer transition state is raised by substrate deuteration that the proton transfer step becomes less rate-limiting and the magnitude of $^{D2O}V/K_{G3P}$ is decreased. This argues persuasively that the primary and solvent kinetic isotope effects are reporting on separate steps, e.g., hydride transfer occurring after alkoxide formation. These data allow us to propose a detailed chemical mechanism for the reaction catalyzed by Mtb-GAPDH.

Chemical mechanism

The chemical mechanism for Mtb-GAPDH shown in Scheme 3 is supported by our determination of the kinetic mechanism, mutagenesis and isotope effect studies. The "free enzyme" is actually present with bound NAD^+, and the two important catalytic

residues, Cys158 and His185, are present as a thiolate-imidazolium ion pair. Binding of glyceraldehyde-3-phosphate yields an initial Michaelis complex, and the Cys158 thiolate nucleophilicially attacks the aldehyde to generate the neutral thiohemiacetal after proton donation from His185. Solvent kinetic isotope effects support a mechanism for oxidation that requires an initial deprotonation of the alcohol to generate the alkoxide that is the largely rate-limiting step. Alkoxide formation promotes hydride transfer from C1 of the covalently-bound G3P thiohemiacetal to NAD^+. This generates the covalently-bound thioester and NADH. Nucleotide exchange and inorganic phosphate binding set up the second half-reaction, the phosphorolysis of the thioester to generate the high energy mixed carboxy-phosphoric anhydride of the product 1,3-bisphosphoglycerate (1,3-BPG), which is released in the final step of the catalytic cycle. The thioester and carboxy-phosphoric anhydride are of roughly equal energy, and permit the substrate level phosphorylation reaction catalyzed by GAPDH to drive the subsequent step in glycolysis catalyzed by phosphoglycerate kinase: the formation of ATP and phosphoglycerate from ADP and 1,3-bisphosphoglycerate.

Acknowledgments

We thank Drs. Subray Hegde and Hector Serrano for the assistance in the purification of Mtb-GAPDH. This work was supported by the National Institutes of Health Grant A1060899 to J.S.B.

Appendix A. Supplementary data

Supplementary data associated with this article can be found, in the online version, at http://dx.doi.org/10.1016/j.abb.2013.10.007.

References

[1] Global Tuberculosis Control, World Health Organization. <http://who.int/tb/publications/global_report/en/index.html>, 2011.
[2] A.H. Romano, T. Conway, Res. Microbiol. 147 (1996) 448–455.
[3] H.L. Segal, P.D. Boyer, J. Biol. Chem. 204 (1953) 265–281.
[4] R.E. Moellering, B.F. Cravatt, Science 341 (2013) 549–553.
[5] M. Perucho, J. Salas, M.L. Salas, Eur. J. Biochem. 81 (1977) 557–562.
[6] Y. Zhou, X. Yi, J.N.B. Stoffer, N. Bonafe, M. Gilmore-Hebert, J. McAlpine, S.K. Chambers, Mol. Cancer Res. 6 (2008) 1375–1384.
[7] L. Zheng, R.G. Roeder, Y. Luo, Cell 114 (2003) 255–266.
[8] H. Kumagai, H. Sakai, J. Biochem. 93 (1983) 1259–1269.
[9] J. Andrade, S.T. Pearce, H. Zhao, M. Barroso, Biochem. J. 384 (2004) 327–336.
[10] P. Rawat, S. Kumar, N. Sheokand, C.I. Raje, M. Raje, Biochem. Cell Biol. 90 (2012) 329–338.
[11] H. Tajima, K. Tsuchiya, M. Yamada, K. Kondo, N. Katsube, R. Ishitani, NeuroReport 10 (1999) 2029–2033.
[12] C. Nicholls, H. Li, J.-P. Liu, Clin. Exp. Pharmacol. Physiol. 39 (2012) 674–679.
[13] I.E. Ichetovkin, G. Abramochkin, T.E. Shrader, J. Biol. Chem. 272 (1997) 33009–33014.
[14] R. Higuchi, B. Krummel, R. Saiki, Nucleic Acids Res. 16 (1988) 7351–7367.
[15] S. Ladame, M. Willson, J. Périé, Eur. J. Org. Chem. 2002 (2002) 2640–2648.
[16] R. Kitz, I.B. Wilson, J. Biol. Chem. 237 (1962) 3245–3249.
[17] W.E. Karsten, C.-J. Lai, P.F. Cook, J. Am. Chem. Soc. 117 (1995) 5914–5918.
[18] L. Liu, W. Huskey, Biochemistry 31 (1992) 6898–6903.
[19] P. Harrigan, D. Trentham, Biochem J. 135 (1973) 695–703.
[20] L. Polgár, Eur. J. Biochem. 51 (1975) 63–71.
[21] S. Moniot, S. Bruno, C. Vonrhein, C. Didierjean, S. Boschi-Muller, M. Vas, G. Bricogne, G. Branlant, A. Mozzarelli, C. Corbier, J. Biol. Chem. 283 (2008) 21693–21702.
[22] D. Trentham, Biochem. J. 122 (1971) 71–77.
[23] J. Jenkins, J. Tanner, Acta Crystallogr. Sect. D 62 (2006) 290–301.
[24] A. Soukri, A. Mougin, C. Corbier, A. Wonacott, C. Branlant, G. Branlant, Biochemistry 28 (1989) 2586–2592.
[25] T. Skarżyński, A.J. Wonacott, J. Mol. Biol. 203 (1988) 1097–1118.
[26] J.D. Hermes, C.A. Roeske, M.H. O'Leary, W.W. Cleland, Biochemistry 21 (1982) 5106–5114.